Characterization of a Continuously Cooled Dual-Phase Steel Microstructure

F. FARIAS, M. BALBI, M.N. BATISTA, and I. ALVAREZ-ARMAS

Continuous-cooling transformation behavior of a DP steel was analyzed from dilation curves with cooling rates that range between 10 °C/s and 98 °C/s and data taken in 10 °C/s increments. For a precise understanding of the problem, several metallographic techniques were used in order to determine which phases and types of transformation are present, the grain structure and crystal defects generated for each cooling rate, among other characteristics. The local distribution of the main alloying elements was analyzed by wave dispersive spectroscopy. From the dilation curves, the relative amount of transformed phase was estimated, as well as the first derivatives as a function of both temperature and time to analyze the characteristics of the transformation and correlate these with a characteristic microstructure. To further understand these results, the mobility of suitable alloying elements such as Cr, Mn, Al, and P was evaluated. The analysis showed that at lower cooling rates, 10 °C/s to 20 °C/s, the transformation occurs at temperatures above 700 °C (at which the majority of alloying atoms have good mobility) in a relatively slow process producing polygonal ferrite. At cooling rates greater than 40 °C/s, the transformation occurs below 700 °C in a relatively short time, where massive transformation takes place. Finally, a cooling rate of 30 °C/s gives a mixed transformation, producing an appreciably smaller grain structure with a high density of crystal defects.

https://doi.org/10.1007/s11661-018-4954-z

I. INTRODUCTION

DUAL-PHASE steels (DP steels) are low-alloy steels that consist of martensite islands embedded in a ferrite matrix. Typically, the martensite volume fraction is about 15 to 25 pct, although small amounts of bainite, pearlite, and retained austenite may also be present. They have a low yield to tensile strength ratio, continuous yielding and a high initial work-hardening rate.

Basically, these steels are manufactured from a simple elemental composition of 0.08 to 0.2 wt pct C, 0.8 to 1.5 wt pct Mn, and 0.2 to 0.5 wt pct Si through intercritical annealing in the $\alpha + \gamma$ region followed by sufficiently rapid cooling to enable the carbon-rich austenite to transform to martensite. Thus, through a relatively simple processing route and lean alloy chemical composition, this steel develops a dual-phase microstructure that provides a wide range of excellent mechanical properties.

Although the production processes for this steel easily form a typical microstructure, the literature includes several papers where different combinations of chemical compositions are tried, in order to improve hardenability and thus mechanical properties.[1–7]

Regardless of the processing route, suitable information about the interplay of chemical composition and processing variables, such as cooling rate, in combination with the resulting microstructure is mandatory. The continuous-cooling transformation (CCT) curves of steels systematically describe the relationships between the cooling rate, phase transformations and microstructure. The CCT curves are the practical standard to determine the results of metal forming and its associated heat treatment processes. Thus, the measurement of CCT curves and phase transformations is very important for material researchers and mechanical engineers in order to design manufacturing processes. In this research, the effects of the alloying elements' redistribution at specific cooling rates, products of the phase transformations and the CCT diagrams' shape were investigated. The aim of this investigation was to characterize a dual-phase steel containing additions of $P + Si > 0.30$ wt pct and $Nb + Ti < 0.01$ wt pct using different metallographic techniques to evaluate the microstructure formed over a wide range of continuous cooling rates.

F. FARIAS, M. BALBI, M.N. BATISTA, and I. ALVAREZ-ARMAS are with the Instituto de Física Rosario IFIR-CONICET, Universidad Nacional de Rosario, Argentina, Bv. 27 de Febrero 210 bis, 2000 Rosario, Argentina. Contact e-mail: farias@ifir-conicet.gov.ar
Manuscript submitted December 4, 2017.
Article published online October 16, 2018

II. EXPERIMENTAL PROCEDURE

A. *Material*

The material studied was a hot-rolled DP-steel in the form of 5.3-mm-thick plates. The steel, provided by TERNIUM SIDERAR, Mexico, had a chemical composition of: $C < 0.12$ wt pct; $P + Si > 0.30$ wt pct; $Nb + Ti < 0.01$ wt pct and trace amounts of Mn, Cr, Al, Ni. Figure 1 shows the initial microstructure of the DP steel, which is composed of 30 pct martensite in a ferrite matrix.

To determine the tensile properties of the material, mechanical tests were performed with an Instron 3382 universal testing system using specimens machined to the E 8M-04 standard. The principal longitudinal monotonic tensile properties in the as-received condition are as follows: YS = 370 MPa, TS = 620 MPa, a uniform elongation (elongation up to the point of necking) of about 24 pct and a total elongation that ranged between 40 and 48 pct, which is notably higher than values reported in the literature for commercial steels.

B. *Dilatometry and CCT Curves*

According to Andrews[8] analysis, the transformation temperatures of the intercritical region of this steel are Ac1 = 722 °C and Ac3 = 860 °C. The continuous-cooling temperature curves (CCT curves) were determined from dilatometry tests performed on a Gleeble 3500 thermomechanical test system. Rectangular slabs of 10 mm wide and 100 mm long were cut using the full plate thickness, heated to 910 °C at a rate of 5 °C/s, soaked for 5 minutes and cooled at 10 °C/s increments between rates of 10 °C/s and 80 °C/s using nitrogen as a refrigerant when needed.

To achieve a cooling rate higher than 80 °C/s, a Bähr DIL 805 A high-speed dilatometer was employed. In this case, a thin-wall tube specimen 10 mm long and 4 mm in diameter with a wall thickness of 1 mm was used to maximize the contact surface with the refrigerant (*N*).

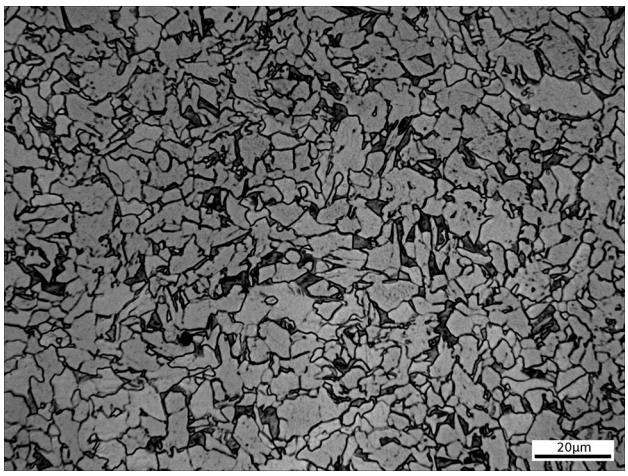

Fig. 1—Bright field OM micrograph showing the as-received DP steel microstructure.

C. *Microstructure Characterization*

In order to analyze the microstructure formed during the cooling tests, the samples were first prepared for EBSD analysis and then for SEM observation by standard mechanical grinding and polishing procedures, finishing with colloidal silica. EBSD experiments were conducted in a FEI Quanta200 SEM equipped with a field emission gun (FEG). Data were analyzed using the EDAX-TSL OIM Analysis software package, which gives the grain size, grain shape and grain/subgrain boundary character, allowing for differentiation between high and low angle boundaries. In the present investigation, the ASTME112 norm was selected to measure grain size, with a minimum misorientation angle of 15 deg. In order to assess this threshold angle, grains with a minimum misorientation of 5 deg were also evaluated (these results will be discussed to validate the 15 deg choice). The Image Quality, IQ, map and the associated numerical data were also used to evaluate lattice defect density after certain cooling rates.

Finally, the samples were etched with a nital (3 pct) + picral (4 g picric acid + 100 mL ethanol) solution and the resulting microstructure was studied in a scanning electron microscope with a secondary electron detector.

D. *X-ray Technique*

To detect retained austenite in the specimens subjected to the CCT tests, X-ray diffraction patterns were measured using Cu-Kα1/Kα2 lines in a Philips X-pert pro MPD goniometer at 40 kV and 30 mA. The scans were carried out from 30 to 85 deg, in 0.02 deg 2θ steps with a 5-second collecting time per step. The instrumental standard chosen to account for instrumental broadening was NIST LaB6.[9] X-ray characterization of each sample was performed by Rietveld refinement[10] of the corresponding patterns, using the Java-based software Maud (Materials Analysis using Diffraction) version 2.55 released April 30, 2015.[11,12]

E. *Wavelength-Dispersive X-ray Spectroscopy (WDS)*

In order to study elemental proportion in different regions, a wavelength-dispersive X-ray spectrometer mounted on an EPMA-JEOL-JXA 8230 scanning electron microscope was used. The EPMA-WDS analysis was performed on spot mode of 3 μm size, with an accelerating voltage of 15 kV, a probe current of 10 nA and a working distance of 11 mm. The specimen preparation technique was analogous to the SEM-EBSD: grinding and polishing up to colloidal silica, finishing with a light nital (2 pct) etching, to allow grain identification.

III. RESULTS AND DISCUSSION

A. *CCT Curves*

Continuous-cooling temperature curves for cooling rates ranging from 10 °C/s to 98 °C/s are shown in Figure 2. The transformation temperatures, defined as

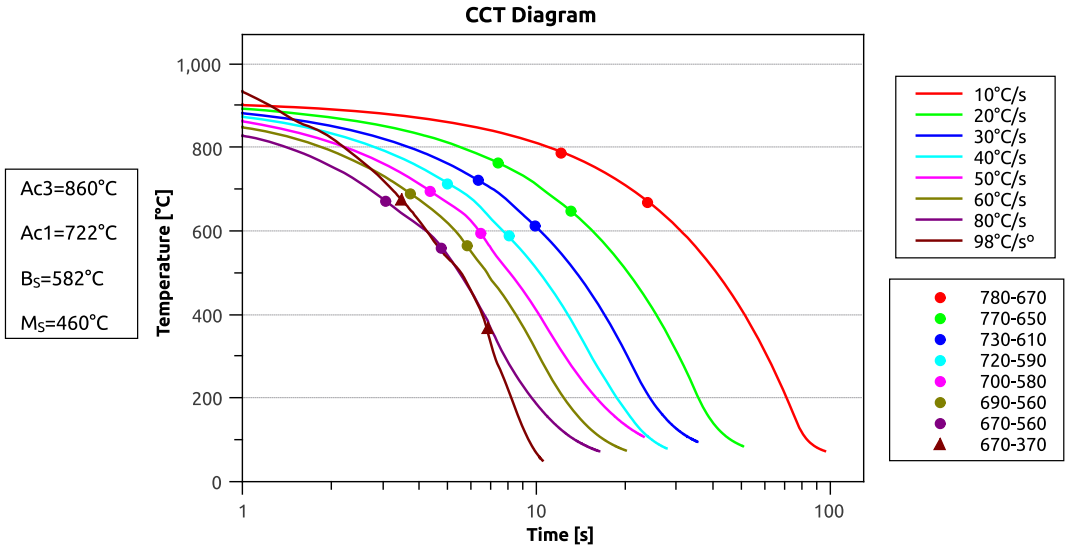

Fig. 2—Continuous-cooling temperature curves for the present DP steel. The legend indicates the temperature ranges over which the transformation occurs.

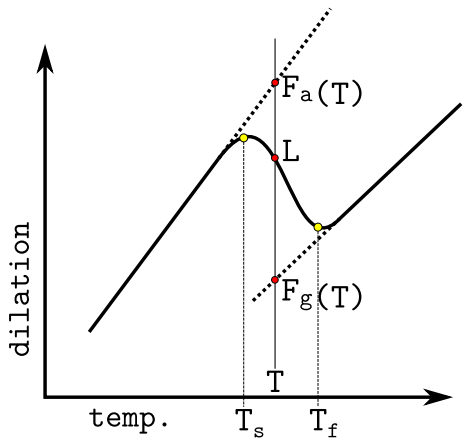

Fig. 3—A dilation-temperature plot for a cooling curve.

those values where approximately 0.2 pct of the material has overcome a phase transformation (99.8 pct for T_f), are given in the graph's legend. The bainite start temperature B_s = 582 °C was calculated using the equation derived by Kirkaldy and Venugopalan.[13] The martensite start temperature, M_s = 460 °C, was obtained using the formula proposed by Kung and Rayment,[14] which is based on a modification of the original linear formula by Andrews. The phase proportion as a function of temperature was calculated from the dilatometry tests using the classic lever rule with a simple Gnuplot script as follows: the ferritic and austenitic dilation *vs* temperature curve, called $F_a(T)$ and $F_g(T)$ respectively, was fitted in the corresponding ferritic ($T < T_s$) and austenitic ($T_f < T$) region and extrapolated to the transformation zone ($T_s < T < T_f$). Then, given that (L, T) are measured values, the austenite fraction is calculated as $\frac{F_a(T)-L}{F_a(T)-F_g(T)}$. Figure 3 illustrates the quantities input to the calculation.

B. *Microstructure Characterization*

Figure 4 shows SEM micrographs of the ferritic structure and other constituents: at 10 °C/s coarse and fine cementite; at 20 °C/s there are, beside cementite particles, regions of degenerated pearlite (cementite plates irregularly arranged or cementite clusters) and occasionally zones with lamellar pearlite; at 30 °C/s there are coarse and fine cementite particles. For cooling rates beyond 40 °C/s, the material develops acicular ferrite or Widmanstätten ferrite, as seen in Figures 4(d) and (e) at; At 80 °C/s some martensitic colonies lying among the previously mentioned constituents/features can be observed.

The dilatometry tests at 98 °C/s were not studied by SEM because the cooling rate of 80 °C/s already produces a ferrite + martensite; thus, it is expected an increase of martensite phase proportion for higher cooling rates.

As can be seen, for cooling rates greater than 40 °C/s, there are no remarkable microstructural changes except for martensite colonies formed at 80 °C/s. This behavior corresponds (for cooling rates ranging from 40 °C/s to 70 °C/s) to a so-called massive phase transformation and will be discussed later.

In order to detect different phases, the specimens were analyzed by X-ray diffraction. These results show that, except for the slowest cooling rate, 10 °C/s, the material progressively retains some austenite as the cooling rate increases. Table I gives these values as measured by the Rietveld method using X-ray diffraction data. The analyzed peaks were (111), (200), (220) for retained austenite and (110), (200), (211) for ferrite. No other peaks were identified in the spectrum. This is related to the fact that due to the low alloying element content, the material does not form carbides at any cooling rate, or at least the quantity is lower than 1 pct.

As will be discussed later, at the lowest cooling rates, 10 °C/s and 20 °C/s (where the cooling process takes place over longer times), the reaction practically occurs

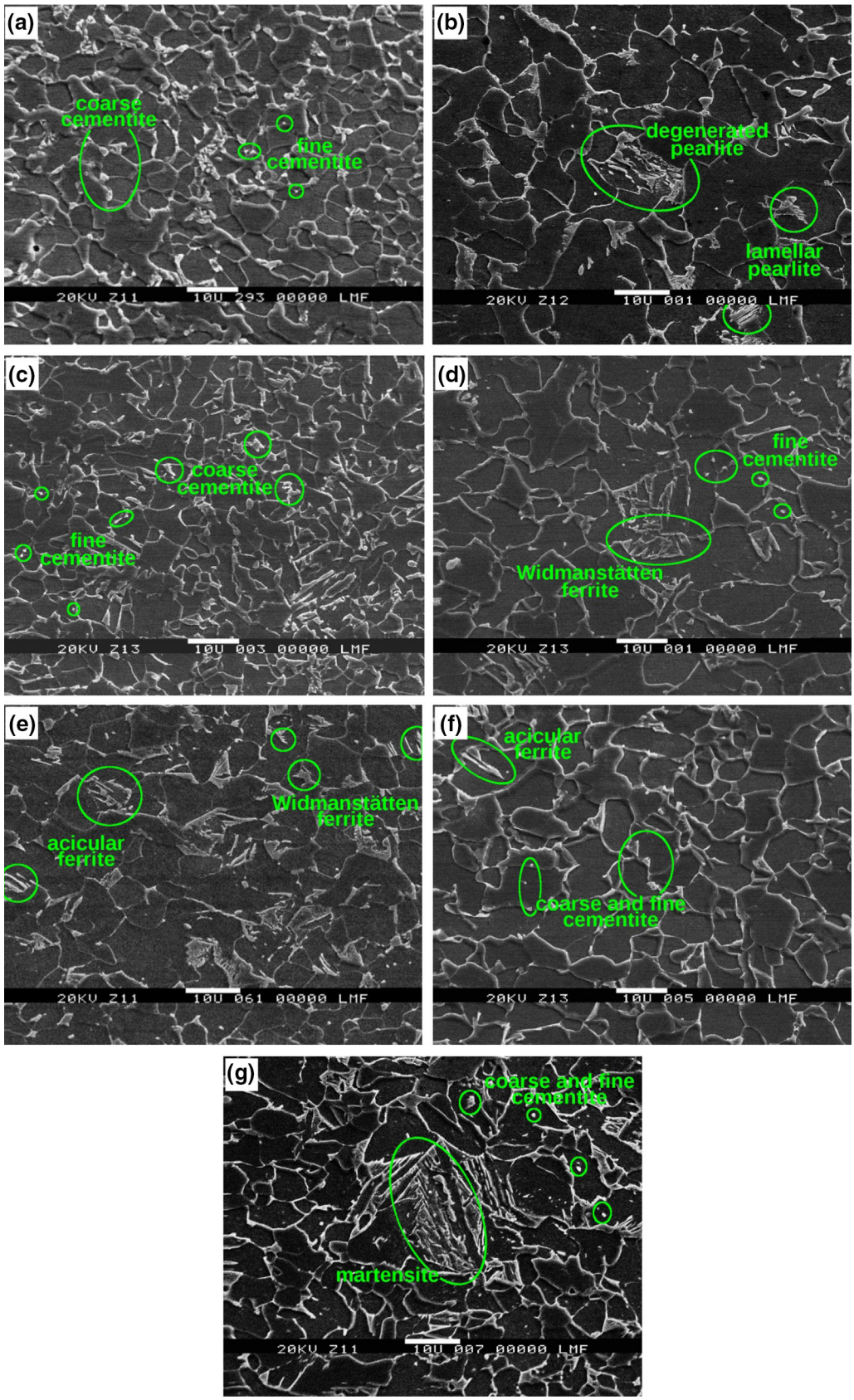
(a)
coarse cementite
fine cementite
20KV Z11 10U 293 00000 LMF
(b)
degenerated pearlite
lamellar pearlite
20KV Z12 10U 001 00000 LMF
(c)
coarse cementite
fine cementite
20KV Z13 10U 003 00000 LMF
(d)
fine cementite
Widmanstätten ferrite
20KV Z13 10U 001 00000 LMF
(e)
Widmanstätten ferrite
acicular ferrite
20KV Z11 10U 061 00000 LMF
(f)
acicular ferrite
coarse and fine cementite
20KV Z13 10U 005 00000 LMF
(g)
coarse and fine cementite
martensite
20KV Z11 10U 007 00000 LMF

◀Fig. 4—SEM micrographs showing the microstructure at: (*a*) 10 °C/s: coarse and fine cementite particles and equiaxed ferrite grain structure; (*b*) 20 °C/s: cementite particles, lamellar and degenerated pearlite and a barely less equiaxed grain structure; (*c*) 30°C/s: coarse and fine cementite particles and a grain structure quite a bit less equiaxed than the previous ones; (*d*) 40 °C/s: small particles of cementite and the formation of a acicular ferrite/ Widmanstätten ferrite within a coarse grain structure; (*e*) 50 °C/s: similar to 40 °C/s; (*f*) 60 °C/s: an equiaxed structure with cementite formation mainly along grain boundaries; (*g*) 80 °C/s: a structure similar to 60 °C/s showing martensite pools within the matrix.

above 700 °C where the austenite transformation is controlled by long-range carbon diffusion as well as diffusion of substitutional atoms including self-diffusion of Fe. Thus, austenite decomposes almost completely to form ferrite, pearlite, cementite particles and eventually cementite plate colonies, due to the relatively slow cooling rate and longer incubation times.

At higher cooling rates, greater than 30 °C/s, the transformation occurs just above 700 °C, and for shorter times below. Thus, an incomplete transformation (such as retained austenite) and displacive transformation mechanisms are observed. Widmanstätten and acicular ferrite formation are displacive in nature and take place at high temperature during shorter times, needing only C diffusion to occur.[15] Moreover, there is general agreement that Widmanstätten ferrite forms at faster cooling rates than polygonal ferrite and in temperature ranges just below those at which equiaxed ferrite forms.

Since the cooling rates of 40 °C/s, 50 °C/s, 60 °C/s, and 80 °C/s produce a microstructure related to displacive mechanisms, the present work will focus on the transition cooling rate, 30 °C/s, which defines a threshold between an intermediate-temperature massive transformation and a high-temperature diffusive transformation.

Wavelength dispersive X-ray spectroscopy (WDS) has the advantage of improved spectral resolution, sensitivity, and the ability to identify even lighter elements than those which can be detected with energy dispersive X-ray spectroscopy (EDS). This technique allowed the spatial distribution of the main alloying elements in the current steel to be studied after the CCT tests. The results showed a homogeneous distribution of Mn, Si and Cr in the matrix for the different cooling rates, Figures 5(a) and (b), and a less homogeneous distribution for Al and P, Figure 5(c). Thus, there is no evidence of micro-segregation of the main alloying elements Mn, Si, and Cr during the transformation while Al and P exhibit some spatial fluctuation. The spatial distribution of C shows a larger variation in concentration for lower cooling rates, 20 °C/s, than for higher rates, 30 °C/s and 40 °C/s, as shown in Figure 5(a). Moreover, a close inspection of these results shows that areas of higher concentration correspond to both cementite particles and pools of retained austenite.

It is evident that solubility plays an important role in the elemental distribution within the steel matrix, indeed, the fact that the elements Mn, Cr and Si are homogeneously distributed means that during soaking in the γ region, they formed a true solid solution. During transformation, the solubility of the ferrite is not surpassed by the concentration of each element and thus, the final structure consists of a fairly uniform solid solution.

Figure 6 shows the Image Quality (IQ) maps corresponding to cooling rates of 10 °C/s, 20 °C/s, 30 °C/s, and 40 °C/s. It is important to remember that IQ maps provide useful visualizations of the microstructure. The contrast in these maps arises from a variety of sources, including phase differences, strain, topography and grain boundaries, among others. Actually, a number of grain boundary allotriomorphs nucleate and grow along parent austenite grain boundaries, as can be seen mostly for cooling rates below 30 °C/s.

In these maps, appear high-angle boundaries (HABs), shown with black lines ($\theta \geq 15$ deg), and low-angle boundaries (LABs), corresponding to orientation difference values less than 15 deg. Figure 7 shows the pronounced increase of LABs produced at a cooling rate of 30 °C/s. These values were taken directly from the IQ data provided by the OIM software.

The average grain size of the specimens cooled at the different rates was calculated using the EBSD analysis and the ASTM E112 standard.[16] Figure 8(a) gives these results for two thresholds, 5 and 15 deg grain angle tolerance. It is worth mentioning that regardless of the grain tolerance values, an important minimum in the curve is observed for the cooling rate of 30 °C/s. In addition to the grain size measurement, the grain shape aspect ratio was also evaluated with the software, as shown in Figure 8(b). This parameter helps in visualizing the non-equiaxed/asymmetry of the ferritic grains, which is important in order to analyze the process of CCT. The graph clearly shows an increase in the frequency distribution of a grain aspect ratio between 0.2 and 0.4 at a cooling rate of 30 °C/s.

Table I. Proportion of Retained Austenite Measured for Different Cooling Rates Using the Rietveld Method

Sample	BCC Phases (Wt Pct) ± 0.5	a-BCC (Å)	Austenite (Wt Pct) ± 0.5	a-FCC (Å)
10 °C/s	99.5	2.8858	< 1	3.6294
20 °C/s	99.0	2.8858	1.0	3.6262
30 °C/s	97.1	2.8853	2.0	3.6267
40 °C/s	97.5	2.8854	2.5	3.6271
50 °C/s	97.1	2.8862	2.1	3.6294
60 °C/s	97.8	2.8892	2.2	3.6295
80 °C/s	97.3	2.8894	2.7	3.6284

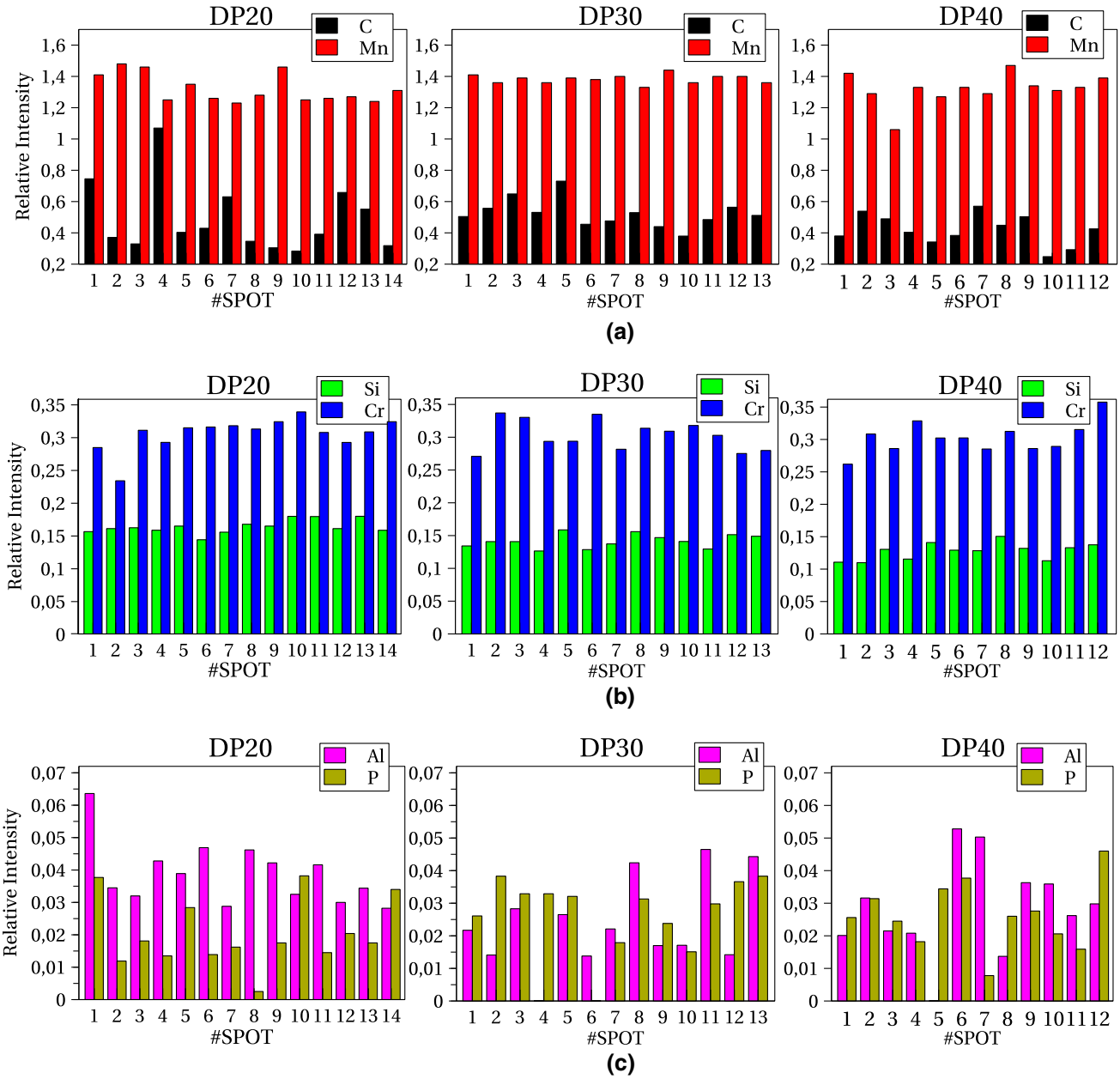

Fig. 5—Wavelength dispersive X-ray spectroscopy (WDS): Spatial distribution and weight percent of (*a*) manganese; (*b*) chromium and silicon; (*c*) aluminum and phosphorous.

As already mentioned, IQ is a good indicator of lattice strain or defect density, relating high strains and lattice imperfections with low IQ values. Moreover, it is frequently used in combination with Confidence Index (CI) data to detect structures with a high density of lattice defects, as is the case for martensite or bainite.[17] For convenience, lower values of the IQ parameter were used to detect the increment of crystal-lattice imperfection produced by the different cooling rates. As a reference, Figure 9(a) shows the complete frequency distribution of the IQ values for 10 °C/s and Figure 9(b) the low IQ values for cooling rates from 10 °C/s to 50 °C/s. There is an appreciable increase of the frequency distribution of low IQ values for rates above 10 °C/s and a more remarkable increase at 40 °C/s and 50 °C/s. This variation of the IQ frequency fraction clearly denotes an increase in dislocation density and other defects as a consequence of the cooling rate.

C. *Transformation by Nucleation and Growth*

The ferrite transformation rate, df_α/dt, as a function of both temperature and time was calculated using the dilatometry test data, (remember that these results combine the nucleation and growth processes). Figure 10(a) shows the $df_\alpha/dt - T$ behavior of the DP

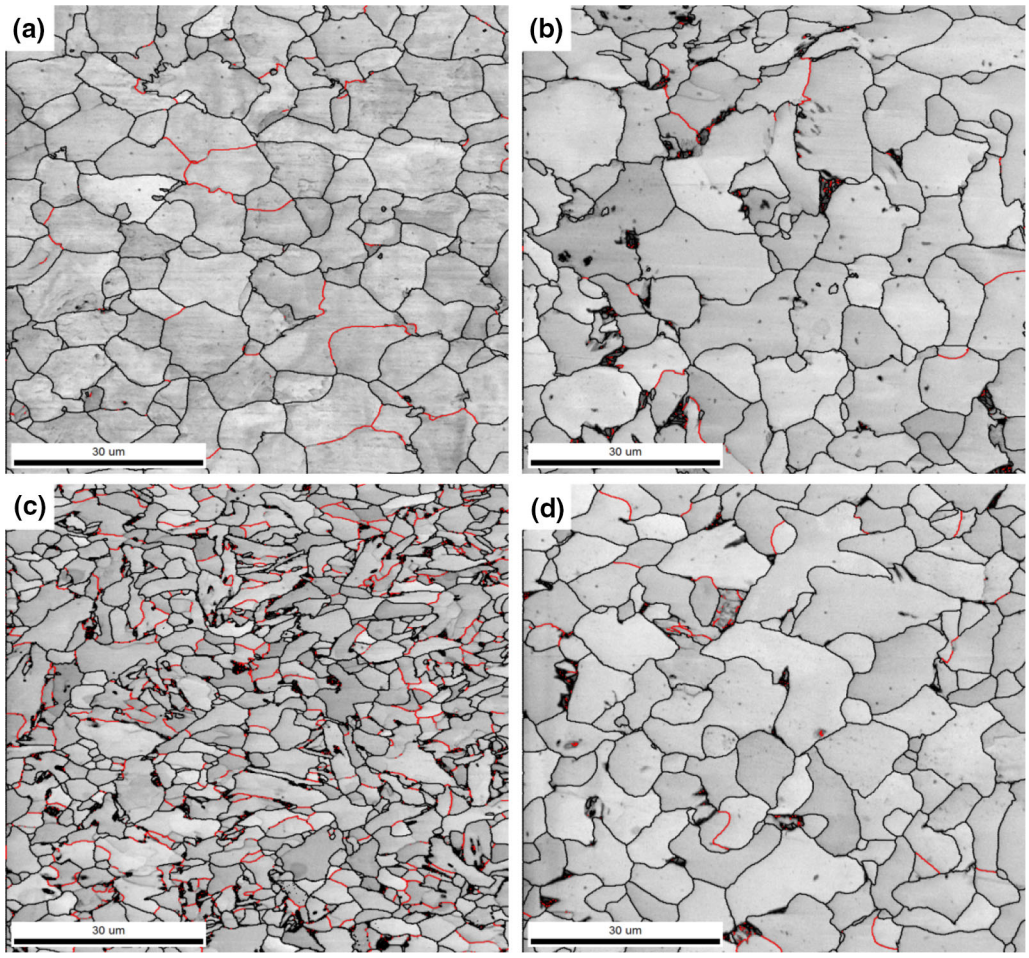

Fig. 6—Image Quality maps: (*a*) 10 °C/s; (*b*) 20 °C/s; (*c*) 30 °C/s; (*d*) 40 °C/s, in which red lines correspond to a boundary rotation angle of $\theta < 15$ deg and black lines to $\theta \geq 15$ deg.

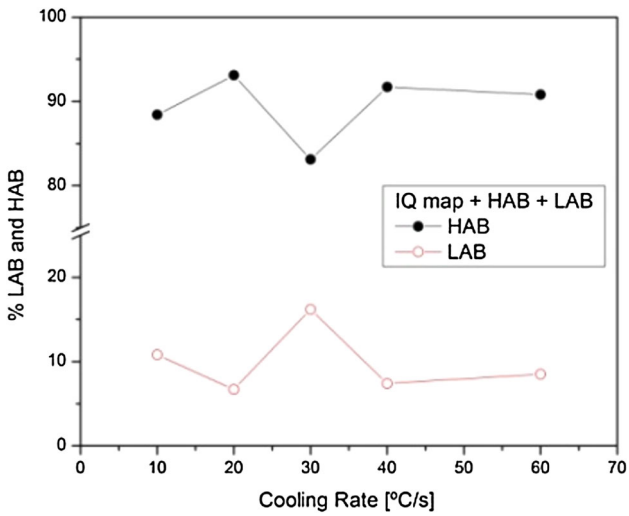

Fig.7—Percentage of high (15 deg $\geq \theta$) and low ($\theta < 15$ deg) angle boundaries.

steel at cooling rates ranging from 10 °C/s to 50 °C/s. The lower cooling rates, 10 °C/s and 20 °C/s, define a range of high-temperature transformation (above 700 °C). Below this threshold, 30 °C/s to 40 °C/s, is an intermediate range of temperatures where the maximum rate of transformation occurs at 680 °C to 690 °C. The γ–α transformation rate below 700 °C is substantially higher than above this temperature. Figure 10(b) shows the process speed. In the high-temperature range, the full transformation is slow and needs several seconds to finish, while at intermediate temperatures the full process is faster, requiring less than 3 seconds to complete. Figure 10(c) details the region at a time of 1 second.

At this point, the steel's microstructural features after cooling over different rates have been described. The most interesting results were obtained for 30 °C/s, where a pronounced decrease of the grain size occurs, as well as the generation of the highest proportion of crystal defects with a high fraction of retained austenite. Consequently, the analysis of these results will be separated in two parts with respect to the cooling rate, namely above and below 30 °C/s which is the transition rate between groups. Also, this cooling rate divides the high and the intermediate temperature ranges in which the ferrite transformation occurs.

The key question is not only how time and temperature affect nucleation and growth of the new phases, but also the role of the undercooling ΔT (driving force

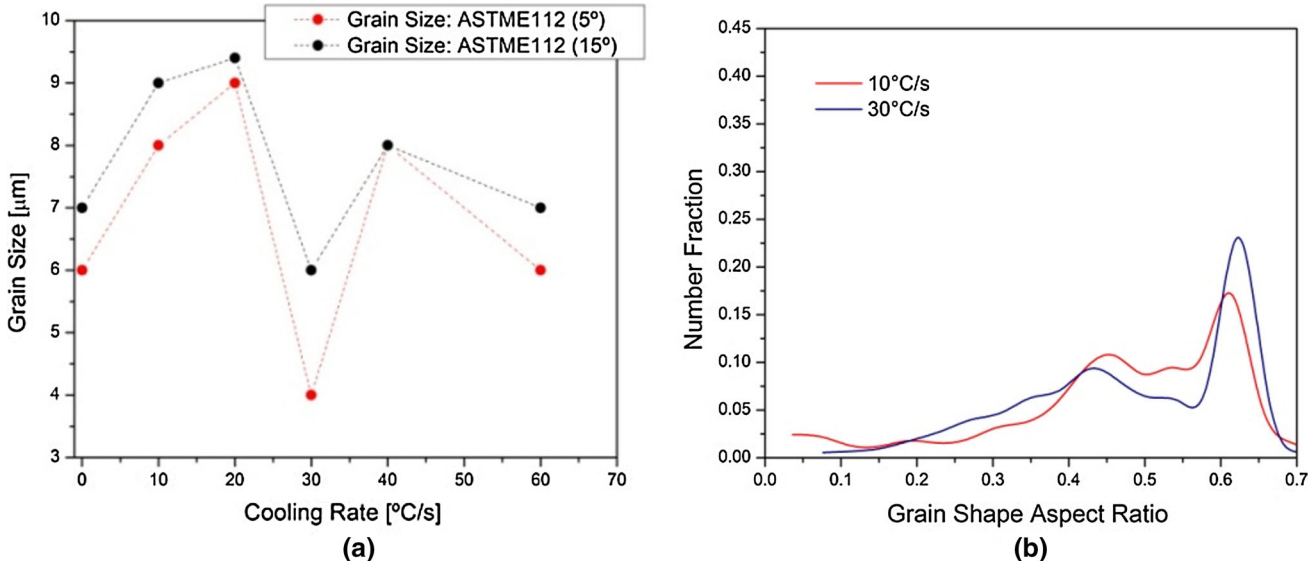

Fig. 8—(*a*) Average grain size for two different grain boundary tolerances, 5 and 15 deg. The dispersion of the values was calculated from the standard deviation of the mean $(SD/(N)^{1/2} = 3$ pct, N: number of grain); (*b*) grain shape aspect ratio.

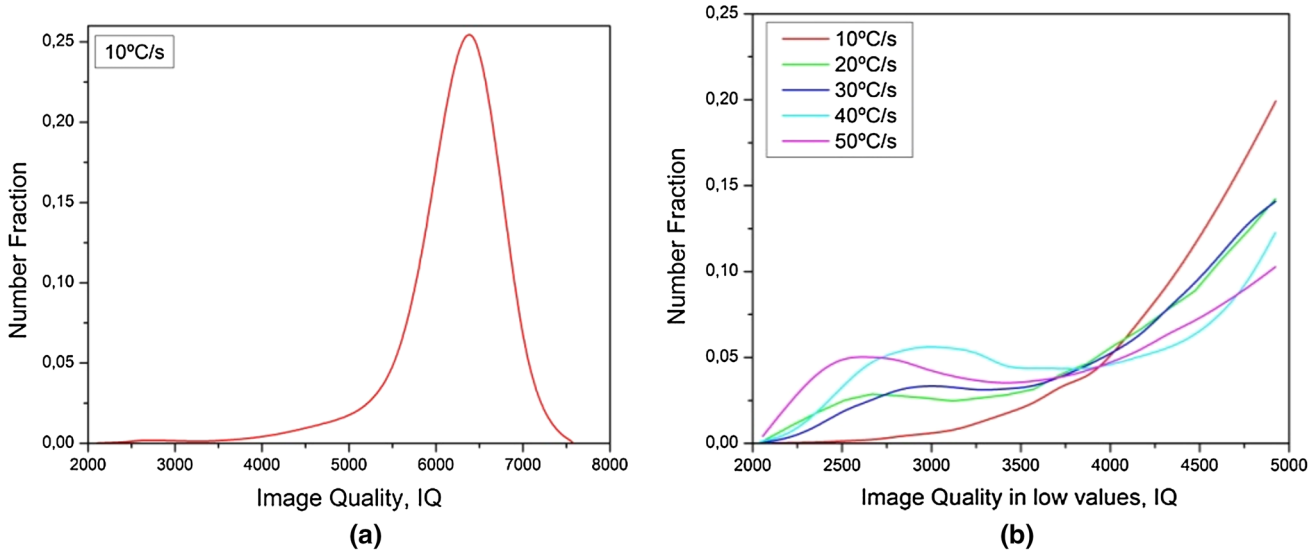

Fig. 9—Distribution frequency of the microstructural Image Quality during continuous-cooling transformation: (*a*) complete frequency distribution for 10 °C/s; (*b*) frequency distribution for lower values of the IQ parameter for cooling rates from 10 °C/s to 50 °C/s.

of the process) on nucleation since nucleation increases with time during the continuous cooling test.

Austenitic grain boundaries are energetically the most favorable sites for the new phase to nucleate, as can be observed by the presence of grain boundary allotriomorphs in Figure 6. Therefore, the phase separation that takes place in the range of intercritical temperatures occurs mostly by a nucleation and growth mechanism (reconstructive transformation). Figure 10(b) indicates not only the duration of the whole process but also the increment of the undercooling, ΔT, for different cooling rates in a fixed time. Figure 10(c) clearly shows that at about one second, the nucleation of stable nuclei has just begun at 10 °C/s, while at 40 °C/s the transformation (nucleation and growth) attains its maximum.

In order to further understand the results, the relation between the transformation rates and the diffusion coefficients for the steel's principal alloying elements are given in Figure 11. Firstly, Figure 11(a) shows the transformation rate curves and the diffusion coefficients of substitutional atoms, *i.e.*, values of self-diffusion of α-Fe in the range 700 °C to 750 °C [18] and the diffusion of Cr[19] and P[20] in an α-Fe matrix between 650 °C to 760 °C. The coefficients of Mn[21,22] and Al[23] were taken at 790 °C because their values were determined for temperatures higher than the Curie value. Notably, the coefficient values of Mn are comparatively lower in the austenite than in the ferrite phase. Si was not included because the temperature at which diffusion starts was determined to be above 900 °C.[21,24] Lastly,

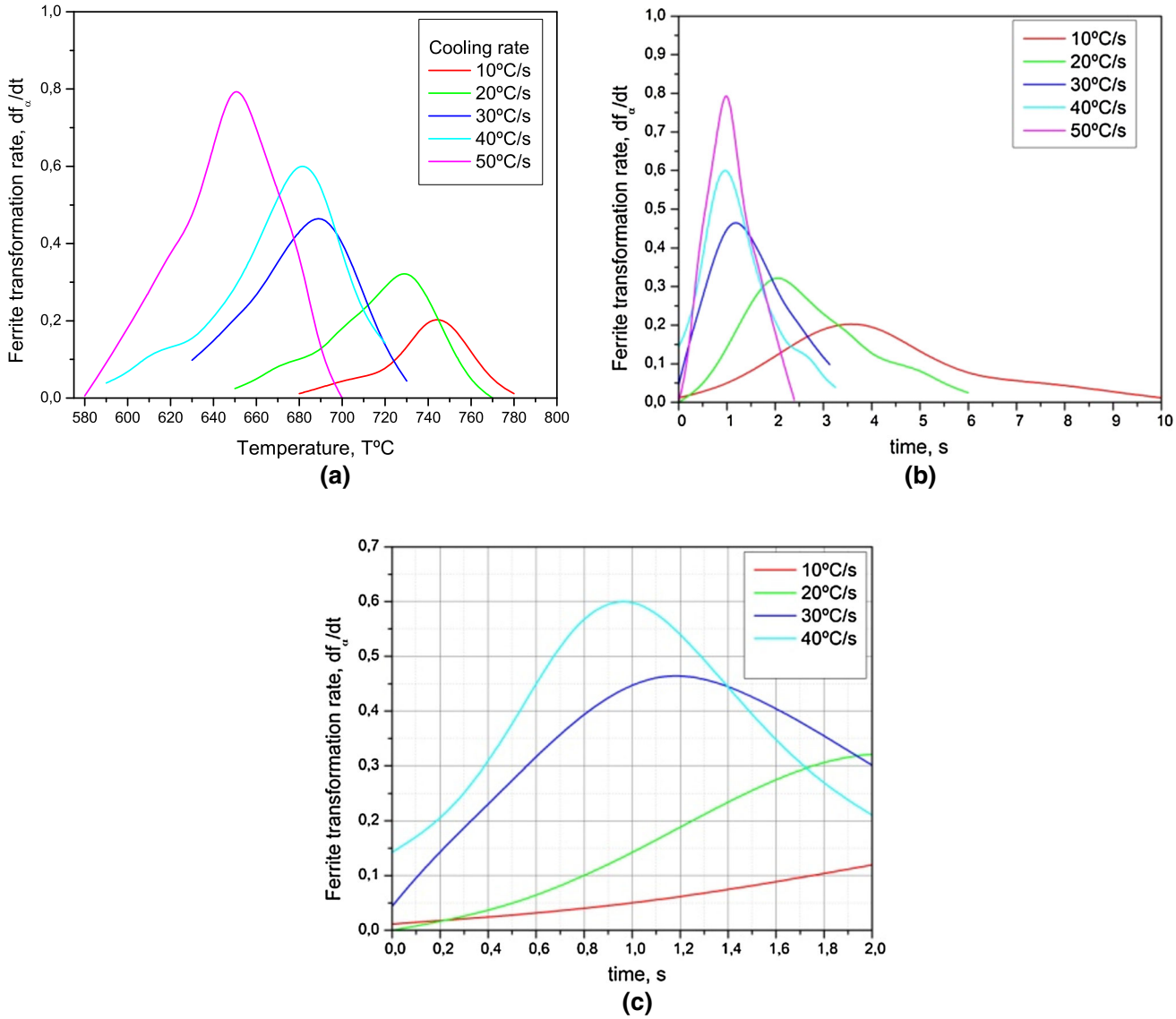

Fig. 10—DP steel: (*a*) ferritic transformation rate *vs* temperature; (*b*) ferritic transformation rate *vs* time; (*c*) magnification of (b) at about 1 s.

Figure 11(b) shows the diffusion coefficient for C atoms in an α-Fe matrix in the range of 450 °C to 720 °C.

During a reconstructive transformation, all elements must diffuse in order to achieve the structural change without the characteristic strains of displacive reactions. However, the temperature range at which the transformation occurs restrains the atoms' ability to move. It is important to remember that time is another important variable for diffusion and during continuous cooling it is limited. Figure 11(c) represents an estimation for the distance that different atom species can move through the lattice in one second. It is worth mentioning that the diffusion coefficient values used in this analysis were taken from data of binary alloys Fe-X, X being the element. According to Bos *et al.*[25] activation energies for interface mobility can be determined by groups of atomic jumps leading to effective activation energies considerably larger than the activation energy for a single atomic jump.

Above 700 °C, where the process lasts several seconds, the coefficients for self-diffusion of Fe and the diffusion of Cr are very close or practically overlap with one another. Thus, it is favorable for both species to jump in order to move α–γ interfaces. On the other hand, below 700 °C, where the transformation occurs in less than two seconds, the mobility of the α–γ interfaces is relatively limited due to the low diffusion coefficients of the main alloying elements.

Growth of polygonal ferrite is controlled by rapid substitutional atom transfer across the austenite-ferrite interfaces and long-range diffusion of carbon atoms rejected from the growing ferrite. For cooling rates of 10 °C/s and 20 °C/s (30 °C/s is the transition rate), it is clear that the growth process (mobility of interfaces) of stable nuclei involves rapid transfer of substitutional atoms (including self-diffusion) across the austenite and ferrite interfaces and long-range diffusion of C rejected from the growing ferrite, Figure 11(b). The favorable

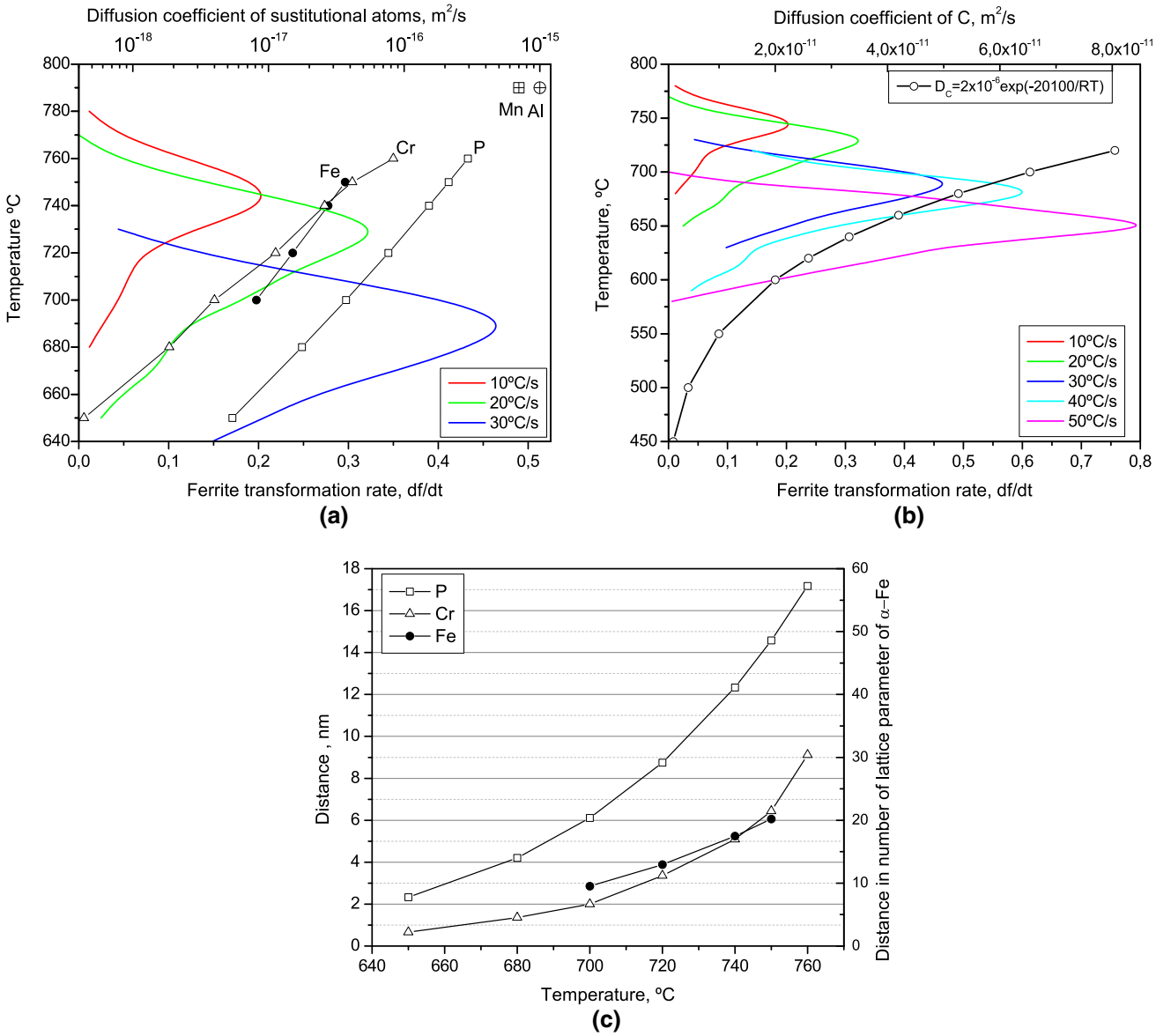

Fig. 11—Relation between ferrite transformation *vs* temperature and (*a*) diffusion coefficient of substitutional atoms in α-Fe; (*b*) diffusion coefficient of C in α-Fe. (*c*) Distance moved by the different substitutional atoms in 1 s. In order to simplify the graph, the lattice parameter of α-Fe was taken as 0.3 nm instead of 0.288 as was measured by X-ray (Table I).

diffusion of some atom species and longer times allows for a reconstructive transformation that minimizes the formation of geometrically necessary dislocations associated with lattice mismatch. This fact is reflected in Figure 9(b), which analyzes the IQ values and the retained austenite proportion given in Table I. Hence, the process is slow enough to allow new grains to grow and form an equiaxed grain structure, and also, some cementite allotropes, Figure 6(b).

At higher cooling rates, self-diffusion of iron atoms loses its importance and even though the diffusion of other species is possible, there is not enough time to complete the process, so the transformation occurs mainly by the diffusion of C. The 30 °C/s cooling rate defines a clear transition in this process, the ferrite transformation starts within the high-temperature region (above 700 °C) and continues through most of the time the alloy is below 700 °C. Physically, this means that the time-dependent undercooling forms a number of stable nuclei that grow as long as the mobility of substitutional atoms is not suppressed, forming a less developed grain structure. This hypothesis is supported by the large number of grain boundary allotriomorphs observed in the microstructure. The structure resulting from this cooling rate contains a high density of dislocations and other lattice defects indicating the activation of a displacive process, at least towards the end of the ferrite transformation.

In summary, at a cooling rate of 10 °C/s, the structure of the steel consists of equiaxed ferritic grains and with a very low retained austenite proportion, less than 1 wt pct. These microstructural characteristics are typical of a long slow high-temperature process.

At 20 °C/s, the ferritic grain structure is somewhat less equiaxed and it contains incipient allotriomorphs with an increasing proportion of retained austenite. However, some evidence of a slow transformation process such as the formation of pearlite was observed. These microstructural characteristics agree with a high-temperature process with insufficient time to complete the transformation.

According to the Dube Morphological System (DMS), the structure obtained during cooling at rates of 10 °C/s and 20 °C/s is termed Polygonal Ferrite (PF) and it is designated as α_p according to the ISIJ Bainite Committee Notation. The equiaxed morphology of the ferrite is characteristic of primary ferrite or a proeutectoid ferrite morphology that precedes pearlite formation in hypo-eutectoid steels. It nucleates and grows along parent austenite grain boundaries and the nucleated crystals are referred to as grain boundary *allotriomorphs*.

At 30 °C/s, the grain structure is quite different from that observed at lower cooling rates, with a smaller, non-equiaxed grain structure and a higher proportion of low-angle boundaries/crystal defects, as well as a high proportion of retained austenite. The characteristics of this grain structure shown in Figure 8 denote a process of nucleation and partial growth of grain boundary allotriomorphs during the transformation. Otherwise, according to Liu *et al.*[26] two extreme growth models can be considered: one for volume diffusion-controlled growth and the other for interface-controlled growth. The former occurs for phase transformation where long-range compositional changes take place while the latter one concerns the case of interface-controlled growth where the growth can occur by atomic processes in the immediate vicinity of the interface. As shown in Figure 11, the γ–α transformation is fast and reaches its maximum extent at a temperature just below that at which equiaxed ferrite forms. Clearly, the transformation process at this rate results in a mixture of microstructures between those characteristics of high and intermediate temperatures, and it is not defined by the Dube Morphological System.

At 40 °C/s, the γ–α transformation is fast and reaches the maximum extent of transformation at 680 °C, Figure 11(a). Regarding the microstructural features, the grain size is coarser than for lower cooling rates, Figure 8(a). Besides, the grain interior shows a high crystal-defect density, as can be seen in Figure 9(b). Finally, there is an appreciable proportion of retained austenite. Therefore, if the cooling process is fast enough, it will prevent the partitioning of carbon between the austenite and ferrite when the steel passes through the ferrite/austenite phase field. This type of transformation is referred to as quasi-polygonal α_q and it is a massive transformation because: (i) there is only a change in crystal structure from FCC to BCC and (ii) no composition changes occur, as there is only a short-range atom transfer across austenite/ferrite interfaces. So, rapid cooling from temperatures where single-phase austenitic microstructures are stable to temperatures where single-phase ferritic microstructures are stable makes possible a high-temperature transformation of austenite to ferrite without a composition change. During this transformation, the change in structure from FCC to BCC causes the formation of crystal defects due to the different austenite and the ferrite lattice parameters.

IV. CONCLUSIONS

The microstructure developed by the DP steel during continuous cooling tests was characterized using different techniques, namely SEM, EBSD, WDS, and X-ray. The following results and conclusions were drawn:

- WDS analysis showed a homogeneous distribution of the main alloying elements Mn, Si, Cr and a non-uniform distribution of Al, P, and C.
- The transformation process can be divided into two stages: (a) A high-temperature stage associated with diffusive process, characterized by a slow transformation rate, which produces an equiaxed grain structure with a low density of crystal defects; (b) an intermediate temperature stage, related to a displacive process that is characterized by a rapid transformation rate, which produces an equiaxed grain structure with a high density of crystal defects.
- The cooling rate of 30 °C/s is a transition rate at which the microstructure firstly forms by nucleation and growth. This is interrupted when the cooling curve passes below 700 °C.

ACKNOWLEDGMENTS

Present work was supported by Agencia Nacional de Promoción Científica y Tecnológica under Grant Number PICT-2014-0341 and Consejo Nacional de Investigaciones Científicas y Técnicas (CONICET) PIP-0426. The authors acknowledge Dr. Roberto Bruna TERNIUM SIDERAR for the donation of the DP steel. As well, the authors acknowledge Dr V. Fuster for the calculation in X-ray technique.

REFERENCES

1. R.G. Davis: *Metall. Mater. Trans. A*, 1979, vol. 10A, pp. 113–18.
2. M.H. Saleh and R. Piestner: *J. Mater. Process. Technol.*, 2001, vol. 113, pp. 587–93.
3. A. Fallahi: *Mater. Sci. Technol.*, 2002, vols. 18–5, pp. 451–54.
4. M. Calcagnotto, D. Ponge, Y. Adachi, and D. Raabe: Effect of Grain Refinement on Strength and Ductility in Dual-Phase Steels. *Proc. 2nd Int. Symp. Steel Sci.* ISSS 2009 Oct 21–24, The Iron and Steel Institute of Japan, Kyoto, 2009.
5. J. Drumond, O. Girina, J.F. da Silva Filho, N. Fonstein, and C.A.S. de Oliveira: *Metallogr. Microstruct. Anal.*, 2012, vol. 1, pp. 217–23.

6. L. Schemmann, S. Zaefferer, D. Raabe, F. Friedel, and D. Mattissen: *Acta Mater*., 2015, vol. 95, pp. 386–98.
7. Y. Granbom: *Structure and Mechanical Properties of Dual-Phase Steels – An Experimental and Theoretical Analysis*, PhD Thesis, Royal Institute of Technology School of Industrial Engineering and Management Materials Science and Engineering, Division of Mechanical Metallurgy, Stockholm, Sweden.
8. W. Andrews: *JISI*, 1965, vol. 203, pp. 721–27.
9. D.L. Kaiser and J.R.L. Watters: *Standard Reference Material®*, 2010, vol. 660b, pp. 721.
10. H.M. Rietveld: *J. Appl. Crystallogr*., 1969, vol. 2, pp. 65–71.
11. L. Lutterotti, S. Matthies, and H.-R. Wenk: *J. Appl. Phys*., 1997, vol. 81, pp. 594–600.
12. L. Lutterotti: Maud (Material Analysis Using Diffraction), 1997.
13. J.S. Kirkaldy and D. Venugopalan: *Phase transformations in ferrous alloys*, TMS-AIME, Warrendale, PA, 1984, pp. 125–48.
14. C.Y. Kung and J.J. Rayment: *Metall. Mater. Trans. A*, 1982, vol. 13A, pp. 328–31.
15. K. Tsuzaki and T. Maki: *J. Phys. IV*, 1995, vol. 5 (C8), pp. 61–70.
16. G. Vander Voort: *Metallography Principles and Practice*, 1st ed., McGraw Hill Inc., New York, 1984, pp. 442–43.
17. M. Calcagnotto, D. Ponge, and D. Raabe: *ISIJ Int*., 2012, vols. 52–5, pp. 874–83.
18. F.S. Bufington, K. Hirano, and M. Cohen: *Acta Metall*., 1961, vol. 9, pp. 434–39.
19. C.G. Lee, Y. Iijima, T. Hiratani, and K. Hirano: *Mater. Trans. JIM*, 1990, vols. 31–4, pp. 255–61.
20. T. Matsuyama, H. Hosokawa, and H. Suto: *Trans. Jpn. Inst. Met*., 1983, vols. 24–8, pp. 589–94.
21. H. Oikawa: *Iron Steel*, 1982, vol. 68 (10), pp. 1489–97.
22. J. Fridberg, L.E. Torndahl, and M. Hillert: *Jernkontor Ann*., 1969, vol. 153, pp. 263–76.
23. H. Amara, C.C. Fu, F. Soisson, and P. Maugis: *Phys. Rev. B*, 2010, vol. 81, pp. 174101-1–174101-11.
24. F.J. Bradshaw, G. Hoyle, and K. Speigh: *Nature*, 1953, vol. 171, pp. 488–88.
25. C. Bos, F. Sommer, and E.J. Mittemeijer: *Acta Mater*., 2005, vol. 53, pp. 5333–41.
26. F. Liu, S.J. Song, F. Sommer, and E.J. Mittemeijer: *Acta Mater*., 2009, vol. 57, pp. 6176–90.